JOURNAL OF Materials CHEMISTRY

Oligopyridine bis(nitronyl nitroxides): synthesis, structures, electrochemical, magnetic and electronic properties

Raymond Ziessel,*[a] Gilles Ulrich,[a] Raphael C. Lawson[b] and Luis Echegoyen*[b]

[a]*Laboratoire de Chimie, d'Electronique et de Photonique Moléculaires, Ecole Chimie, Polymères, Matériaux (ECPM), Université Louis Pasteur (ULP), 25 rue Becquerel, BP08, 67087 Strasbourg Cedex 02, France*

[b]*Department of Chemistry, University of Miami, P.O. Box 249118, Coral Gables, Florida 33124, USA*

Received 24th December 1998, Accepted 15th April 1999

A family of pyridine, 2,2′-bipyridine, 1,10-phenanthroline, 3,6-bis(2-pyridyl)pyridazine ligands bearing two nitronyl nitroxide radicals was synthesized and characterized. The pincer ligands having two radicals in *ortho* positions relative to the nitrogen atoms form stable nickel(II) and copper(II) complexes. The pyridine based 2,6- and 2,5-biradicals crystallized in the monoclinic space group $P2_1/c$ while the bipyridine 5,5′-biradical crystallized in the monoclinic space group $P2_1/n$ (radical is 4,4,5,5-tetramethylimidazoline 3-oxide 1-oxyl). The highest dihedral angle between the radicals and the pyridine ring is found in the pyridine 2,6-biradical (*ca.* 47°), followed by the 2,5-biradical (*ca.* 38°) and then by the bipyridine 6,6′- (*ca.* 27°) and 5,5′-biradicals (*ca.* 24°). All the biradicals exhibit similar EPR spectra, in solution and at room temperature, with nine lines due to coupling of the unpaired electrons with four equivalent nitrogen nuclei (hyperfine coupling constant A_N 3.3–3.8 G). In some cases these nine lines are reduced to five lines (A_N 7.5–7.6 G) at low temperature due to a weakening of the spin–spin exchange interaction J which becomes smaller than the isotropic coupling constant. The χT product for all radicals measured at 300 K lies in the range of 0.70–0.77 emu K mol^{-1}. For the pyridine 2,6- and 2,5-biradicals, magneto-structural correlation reveals through bond ferro- and antiferro-magnetic interaction ($J/k_B = +9.4$ and -39 K, respectively) due to a favorable spin polarization effect. These intramolecular interactions persist when the radicals are dispersed in a polystyrene matrix. For the bipyridine 6,6′- and 5,5′-biradicals, the experimental data were fitted using a Bleaney–Bowers expression for two interacting spins and the values of $J/k_B = -24$ to -1.9 K, respectively, are representative of an antiferromagnetic through-space interaction between two neighboring radicals. No intramolecular magnetic interactions were found in the oligopyridine based compounds. In all of these biradicals, both nitroxides are oxidized at the same potential (*ca.* +0.45 V *vs.* Ag/Ag$^+$) by a two-electron quasi-reversible process to the nitrosonium dication and irreversibly reduced to the dianions between -1.80 and -1.40 V. In the Cu(II) and Ni(II) complexes of the bipyridine-6,6′- and phenanthroline-2,9-biradical reduction of the nitroxides to the hydroxylamine anions is quasi-reversible and is facilitated by *ca.* 1.20 V *versus* the 'free' ligands, and the second redox couple corresponds to reduction of the bridging bipyridine or phenanthroline fragments. In the nickel based complex of the pyridine-2,6-biradical two sets of equivalent nitroxides are successively reduced by a dielectronic process while the monoelectronic reductions of the two bridging pyridines are separated by 330 mV.

Introduction

Pioneered at the end of the 60s by Ullman and co-workers,[1] the nitronyl nitroxide (*N*-oxyl *N*′-oxide) radical family led to no real development in the field of spin labelling, and it was only in the mid-80s that it generated a growing interest from chemists. Gatteschi and co-workers[2] discovered interesting magnetic interactions between nitronyl nitroxides and paramagnetic metal centers, whereupon the nitronyl nitroxide radical family started to be widely used in the field of molecular magnetism. For instance acidic and paramagnetic metal complexes were found to exhibit very interesting magnetic properties with many different molecular arrangements ranging from discrete molecules to cyclic manganese hexamers.[3,4] In the meantime, some nitronyl nitroxide derivatives were also found to order ferromagnetically at cryogenic temperatures such as the γ phase of *p*-nitrophenyl nitronyl nitroxide[5,6] and a diaza-adamantane dinitroxide compound,[7] while thiomethylphenyl[8] or triazole[9] nitronyl nitroxide radicals also display interesting ferromagnetic properties. The specific role played by hydrogen bonds in the crystal packing and in the propagation of ferromagnetic interactions has been discussed for ferromagnets based on polyhydroxyphenyl radicals[10,11] and ethynyl bridged pyridine based radicals.[12] Progress in the development of organomagnetic materials based on nitroxide radicals has recently been highlighted.[13]

The main objective in this field is to obtain co-operative magnetic properties in an organic or organometallic solid. The key element lies in the selection of suitable open-shell molecules and to orient them properly relative to each other in a three dimensional network. In order to avoid the natural preference of molecules for antiparallel spin alignment, structural modifications and chemical functionalization of stable open-shell molecules represent a challenging problem.

As part of our continuing interest in molecular based magnetic materials, and in order to synthesize two- or ideally three-dimensional structures able to display permanent magnetization, we chose as building blocks metal complexes based on chelating molecules possessing organic spin carriers, using a 'complex as ligand/complex as metal' approach. Therefore, we focused on the synthesis of novel oligopyridines bearing two nitronyl nitroxide free radicals symmetrically attached to the chelating core. The use of oligopyridine derivatives offers a strong co-ordinative center, which affords very stable transition metal complexes with a controlled geometry. Exotic

molecular architectures could be built by using these novel chelating biradicals as building blocks that can be connected, one to each other, by acidic metal centers.

As a first step towards this goal, knowledge of the electronic, magnetic and redox properties of such ligands gives important information on the nature of the interactions between the different paramagnetic parts of the molecule. We report here the synthesis, structural characterization, EPR, magnetic and electrochemical properties of a series of spin-labelled oligopyridines and some of their metal complexes.

Results and discussion

Preparation of the biradicals

Formyl compounds, precursors of the nitroxide radicals, were prepared using adapted literature procedures. 2,6-Diformylpyridine was prepared by a Swern oxidation[14] of the corresponding dialcohol. 2,5-Diformylpyridine was prepared by the following sequence of reactions: (i) esterification of the corresponding diacid; (ii) reduction of the methyl diester with $NaBH_4$ to give the dialcohol and (iii) subsequent Swern oxidation to the dialdehyde. This method is an adaptation from those used by Beer and co-workers,[15] for the synthesis of the 4,4′-diformyl-2,2′-bipyridine. The two other symmetric isomers, 5,5′-diformyl-2,2′-bipyridine and 6,6′-diformyl-2,2′-bipyridine, were obtained respectively following the syntheses described by Mendoza *et al.*[16] and Holm and coworkers.[17] 2,9-Diformyl-1,10-phenanthroline was prepared from neocuproine using selenium dioxide.[18] The 3,6-di(6-formyl-2-pyridyl)-pyrazine was prepared by a Swern oxidation of the corresponding dialcohol, itself prepared from 6-cyano-2-hydroxymethylpyridine following the same method as for the synthesis of 3,6-bis(2-pyridyl)pyrazine earlier described by Butte and Case.[19]

The corresponding *N,N*′-dihydroxyimidazolidines **b** were prepared in good yield by multiple condensation of the dialdehydes **a** with 2,3-diamino-*N,N*′-dihydroxy-2,3-dimethylbutane[20] in methanol as sketched in Scheme 1.[21] The precursors of the nitroxide radicals (the bis-hydroxyimidazolidines) precipitate during the condensation step and could be isolated as white powders. During the condensation of the dialdehydes **2a** and **6a** no precipitate was obtained and the mother-liquor was used for the next step. Secondary products formed during the synthesis are due to dehydration of the bis-*N,N*′-hydroxyimidazolidine to *N*-hydroxyimidazoline. This kind of dehydration can be favored by the presence of impurities in the starting dialdehydes, such as selenium dioxide.[22] If the dehydration step is faster than the condensation of the 2,3-diamino-*N,N*′-dihydroxy-2,3-dimethylbutane with the aldehyde function no precipitate of the bis-*N,N*′-hydroxyimidazolidine derivative is obtained. In this case an oxidation of the mother-liquor is necessary to recover the bis(nitronyl nitroxide). Side-products such as the bis(iminonitroxide) and the mono(nitronyl nitroxide) mono(iminonitroxide) are separated by column chromatography.

There are two characteristic peaks in ^{1}H NMR spectrum of the bis-*N,N*′-hydroxyimidazolidine moieties **b**: the hydroxy groups appear between δ 7.6 and 7.8 and the central protons of the imidazolidine structures are identified by a singlet between δ 4.6 and 4.8. In the ^{13}C-{^{1}H} NMR spectra the central carbon of the imidazolidine group appears between δ 89 and 93 (see Table 1 for selected data).

Table 1 Selected spectroscopic data for the bis-imidazolidine compounds

Product	IR ν^a/cm^{-1}	^{1}H NMR (δ)^b	^{13}C-{^{1}H} NMR (δ)^c	Mass^d
1b	3405	4.67	92.5	396
3b	3254	4.75	92.8	473
4b	3254	4.62	89.5	473
5b	3252	4.60	90.7	473
7b	3342	4.81	92.8	551

$^a\nu_{OH}$ measured in KBr pellets. ^{b}Central imidazolidine H atom measured in d_6-DMSO solutions. ^{c}Central imidazolidine C atom measured in d_5-pyridine. ^{d}Obtained by FAB$^+$, corresponds to $[M+H]^+$.

The *N,N*′-dihydroxyimidazolidine intermediates were oxidized in good yields to the nitronyl nitroxide radicals **c** using sodium periodate in a two-phase mixture of dichloromethane and water. Under these conditions the blue or green radicals (Fig. 1) are progressively solubilized in the dichloromethane and no overoxidation occurs during a one hour oxidation. This method was preferred to the use of solid metal

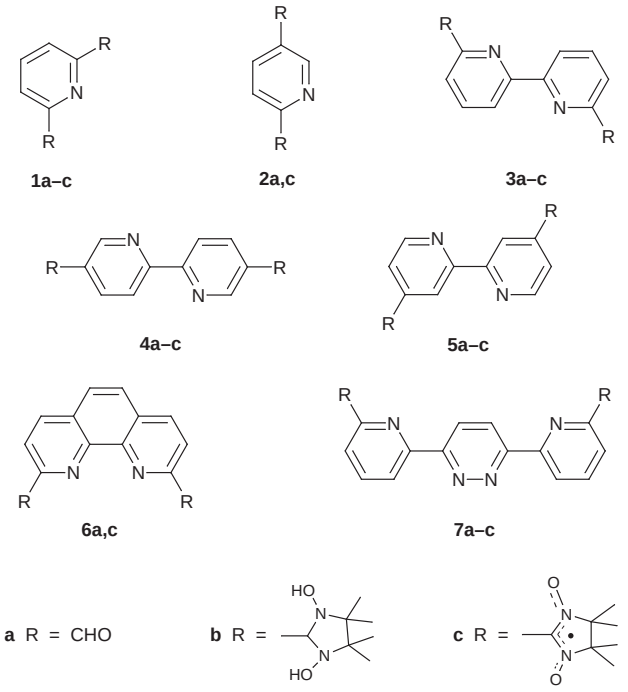

Fig. 1 Structures of the bis(nitronyl nitroxide) radicals **1–7**.

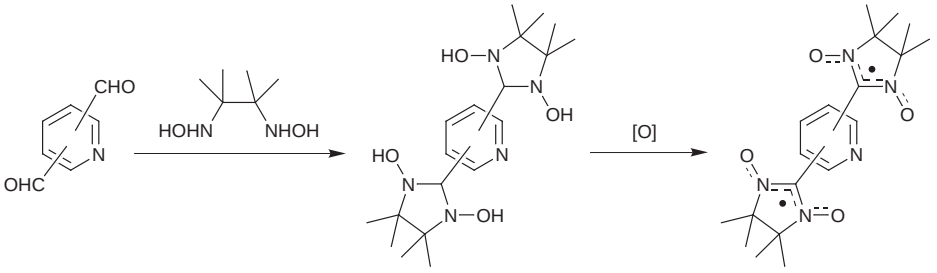

Scheme 1

Table 2 Selected spectroscopic data for the nitronyl nitroxide bis-radicals

Product	IR ν^a/cm^{-1}	UV-Vis λ_{max}/nm (ε/M^{-1} cm^{-1})	Mass^b	EPR A_N^c/G
1c	1368	570(720)	390	3.3
2c	1351	585(550)	390	3.6
3c	1358	575(740)	467	3.8
4c	1347	607(320)/ 532(350)	467	3.8
5c	1354	597/530	469	—
6c	1376	568(610)	491	3.6
7c	1363	574(720)	545	3.8

[a] ν_{NO} measured in KBr pellets except for compound **5c** measured in CH_2Cl_2 solution. [b] Measured in dichloromethane by FAB$^+$, corresponds to $[M+H]^+$ or $[M+2e+3H]^+$ for **5c**. [c] Measured in dichloromethane at room temperature.

oxide, except for the preparation of **2c** where a silver oxide oxidation of the mother-liquor is suitable for the synthesis of the biradical. All the radicals were purified by column chromatography using alumina, and then recrystallized by slow evaporation of dichloromethane from a mixture of *n*-hexane–dichloromethane, except for **5c** which gave a green powder after evaporation of the solvent. This green paramagnetic solid is no longer soluble, even in DMF, and presents most of the characteristics of the nitronyl nitroxide compounds. A solution of **5c**, prior to evaporation, gave the expected FAB$^+$ mass spectrum and corresponding spectroscopic properties. No further structural information concerning the resulting insoluble material has yet been obtained.

The bis(nitronyl nitroxide) derivatives appear very stable in the solid state, and their characteristic dark blue or green color is due to n→π* transitions of the aminoxyl oxides.[23] The FAB$^+$ mass spectra exhibit an intense molecular ion peak (corresponding to $[M+H]^+$), and major characteristic fragments due to the successive loss of oxygen atoms. Most of these compounds decomposed above 200 °C. In the IR region they all show an intense ν_{NO} stretching vibration characteristic of the nitronyl nitroxide subunits (Table 2).[23] Magnetic moments were determined with a SQUID susceptometer and lie in the expected range of 2.37 to 2.48 μ_B.

Complexation studies

Complexation studies were performed with the pincer ligands possessing nitronyl nitroxide subunits in the *ortho* positions of the pyridine fragment (Fig. 2). In this case there is synergistic co-ordination of the central pyridine group and the oxygen atoms of the radicals. Compound **1c** is in this way a potential O_2N tridentate ligand, which allows the preparation of mononuclear copper(II) and nickel(II) complexes with a 2:1 ligand:metal stoichiometry. These compounds have been characterized by FAB$^+$ mass spectrometry and elemental analysis. The co-ordination of the oxygen of the nitronyl nitroxide group is confirmed by a significant shift of the NO stretching frequency (16 and 25 cm^{-1} respectively for the Cu(II) and Ni(II) complexes) and by a significant hyperchromic effect observed for the n→π* electronic transition.

In compounds **3c** and **6c** the presence of two radical subunits in the *ortho* positions of the pyridine gave complexes in which the ligands are tetradentate (O_2N_2 co-ordination mode). Stable complexes of Cu(II), Ni(II), Zn(II), Co(II) and Mn(II) were obtained with **3c** and their synthesis, crystallographic data and magnetic properties are discussed elsewhere.[24] The copper(II) and nickel(II) complexes of **6c** are obtained in a similar manner as for **3c**, and form stable one ligand to one metal complexes. The two pyridines and two nitronyl nitroxides co-ordinate the metal center in an equatorial fashion and the pseudo-octahedral co-ordination is completed, in the axial positions, by

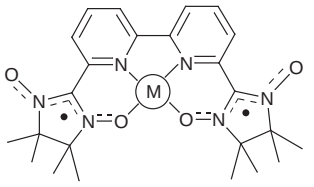

8 : M = $Cu(ClO_4)_2$
9 : M = $Ni(ClO_4)_2$

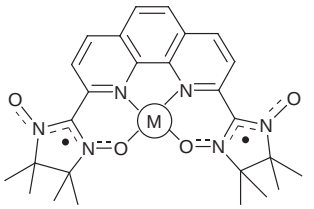

10 : M = $Cu(ClO_4)_2$
11 : M = $Ni(ClO_4)_2$

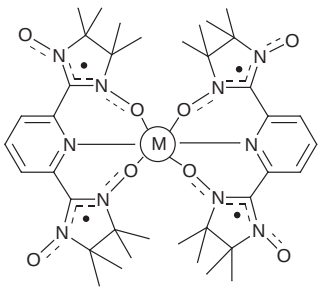

12 : M = $Cu(ClO_4)_2$
13 : M = $Ni(ClO_4)_2$

Fig. 2 Schematic structures of copper(II) and nickel(II) complexes **8–13**.

the perchlorate counter ions and/or solvent molecules. The observed molecular ion peaks in the FAB-MS spectra are respectively at *m*/*z* 654 and 647 for the copper(II) and nickel(II) complexes of **6c** and correspond to the mass of the complex with loss of one perchlorate anion and addition of two protons in the case of the copper complex. The co-ordination of the oxygen of the nitronyl nitroxide group is also confirmed by a significant shift of the NO stretching frequency (25 and 21 cm^{-1} for the Cu(II) and Ni(II) complexes respectively).

Crystal structures of compounds 1c, 2c and 4c

The crystal structure of compound **3c** has previously been reported[25] but not the crystal packing. The intermolecular contacts which may account for the magnetic exchange pathway were investigated herein. Deep blue block crystals for **1c**, **2c** and black-green blocks for **4c** were analysed by X-ray diffraction and ORTEP[26] drawings are given in Figs. 3 and 4.

The molecular structure of compound **1c** (Fig. 3) is similar to the one described by Oshio *et al.*[27] which has a different crystallographic lattice and space group ($P2_1/a$). This different cell organization can be explained by different crystallization conditions. The dihedral angle between the plane of the pyridine ring and the average plane of the C_5 ring is 47°, and the angle between the two average planes of the radical groups is nearly orthogonal [89°, in Fig. 3(a)]. These strong tilt angles are probably due to both electronic repulsion of the free electron with the lone pair of the nitrogen atom and steric crowding. The same electronic interaction is present in **3c**, but steric congestion is less severe resulting in a significant decrease of the tilt angle (see above). Adjacent radicals are organized in a head-to-tail fashion to form dimers belonging to the *ab*

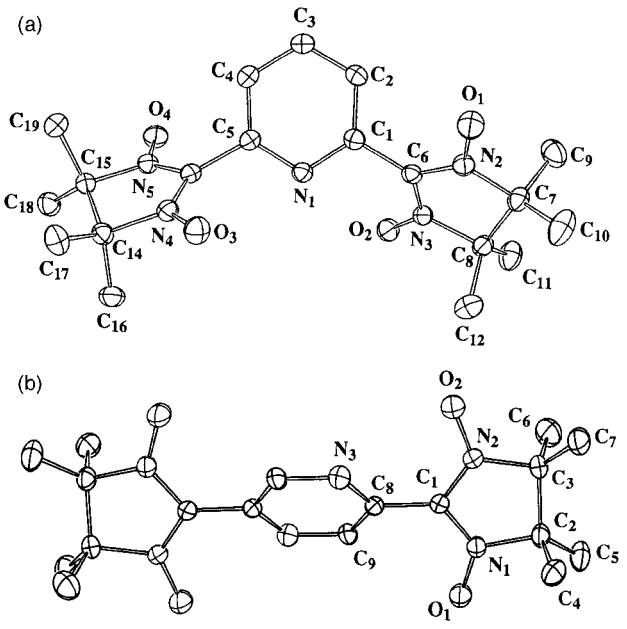

Fig. 3 ORTEP views of compounds **1c** (a) and **2c** (b).

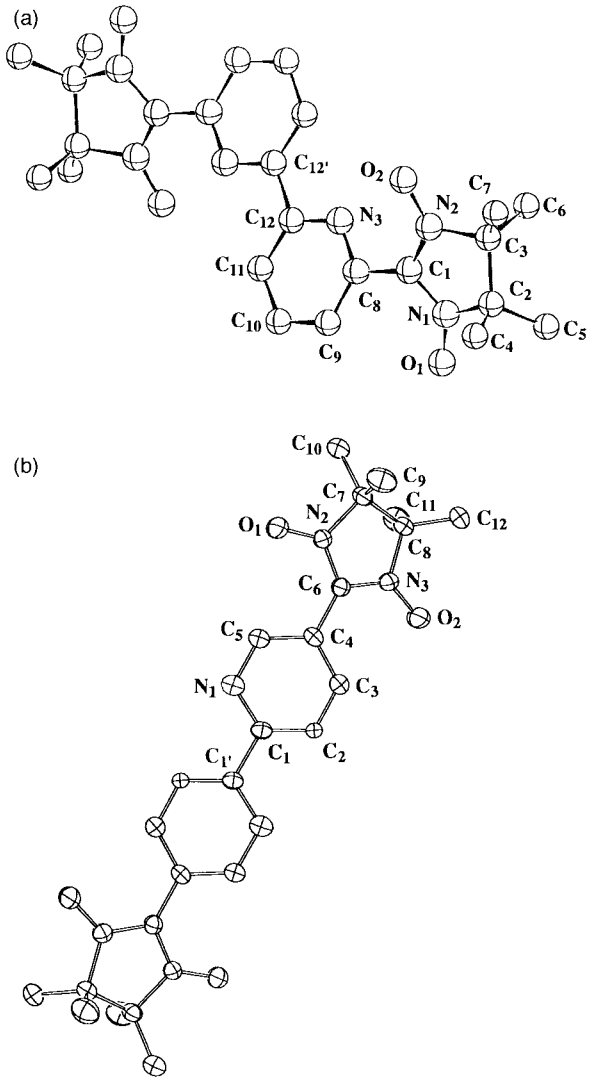

Fig. 4 ORTEP views of compounds **3c** (a) and **4c** (b).

plane, with a O4···O4′ distance of 3.14 Å and O4···N5′ of 3.76 Å. Indeed, intermolecular interaction in two radicals oriented in a head-to-tail fashion is at the maximum when the two NO groups are arranged in such a way that the O–N···O′ angle α is equal to 90° and the angle β between the π^* orbitals of the nitronyl nitroxide radicals with a vector normal to the N_2O_2 plane is also 90°.[28] Here the angles $\alpha \approx 52°$ and $\beta \approx 90°$ are in keeping with antiferromagnetic interactions which owing to the large NO···NO distances are predicted to be weak. The dimer is isolated from its neighbor with distances larger than 8 Å (Fig. 5).

For compound **2c** the position of the pyridine could not be determined exactly due to the presence of an inversion center in the middle of the pyridine ring, while an angle of *ca.* 38° between the average plane of the radicals and the pyridine is observed [Fig. 3(b)]. In the present structure the distances between the N–O and C–N atoms of the radical subunits are similar: N(1)–O(1) 1.277(2); N(2)–O(2) 1.275(2); C(1)–N(2) 1.331(3); C(1)–N(1) 1.356(3) Å. This symmetry is due to the complete delocalization of the odd electron in the non-bonding orbitals of the 'ONCNO' core. The N–O bond distances are between the values of a single and a double N–O bond and the C–N bond distances are near the value of a double bond. It is reasonable to expect that the spin density is mostly localized on the N–O bonds as previously observed by polarized neutron diffraction.[29] Examination of the crystal packing shows that the radicals lies at relatively large distances O1···O1′ 5.77 Å (Fig. 6) with geometrical parameters O1···N2′ 5.66, O2···N1′ 6.04 Å, O–N···O′ angles $\alpha \approx 80°$ and $\beta \approx 80°$. The long radical–radical distance found in **2c** is not favorable for efficient magnetic interactions.

As expected, the free biradical **3c** has a transoid arrangement of the two pyridine rings with a center of symmetry located in the middle of the bipyridine C–C bond. The two pyridine rings are coplanar and form an angle of 27° with the mean plane of the imidazolidine subunit [Fig. 4(a)]. Close examination of the crystal packing shows that the N–O entities of neighboring molecules are arranged in a head-to-tail fashion forming crystallographic chains along the *c* axis (Fig. 7), and at intermolecular distances short enough to favor magnetic interactions. Relevant intermolecular geometrical data are: O1···N1′ 3.70, O1···O1′ 3.78, O–N···O′ angles $\alpha \approx 84°$ and $\beta \approx 90°$. The shortest interchain distances are 3.51 (O1···C4′) and 3.54 Å (O2···C10′) while the shortest interchain NO distance is 6.64 Å.

Compound **4c** also crystallized in a transoid arrangement, with an inversion center of symmetry located in the middle of the C–C bond [Fig. 4(b)]. The bipyridine is planar and there is a dihedral angle between the mean plane of the C_5 ring and the pyridine of 24°. The N2–O1 1.28, N3–O2 1.28, C6–N2 1.34 and C6–N3 1.35 Å bond distances are similar. Here also close examination of the crystal packing shows that the N–O entities of neighboring molecules are arranged in a head-to-tail fashion forming crystallographic chains along the *b* axis (Fig. 8) and at intermolecular distances short enough to favor magnetic interactions. Relevant intermolecular geometrical data are: O1···N1′ 4.15, O1···O1′ 3.01 Å, angles $\alpha \approx 22°$ and $\beta \approx 14°$. The shortest interchain distance is 3.49 Å (C1···C11′), while the shortest interchain NO distance is 5.34 Å.

EPR properties

The room temperature EPR spectra of these compounds obtained in dichloromethane solution are all characteristic of bis(nitronyl nitroxide) systems with strong intramolecular spin–spin interaction. Nine spectral lines are observed due to coupling of the delocalized unpaired electrons with four equivalent ^{14}N nuclei. The hyperfine coupling constants (A_N) given in Table 2 lie between 3.3 and 3.8 G. Interestingly, the nine lines observed at room temperature for compounds **1c**, **2c**, **3c**,

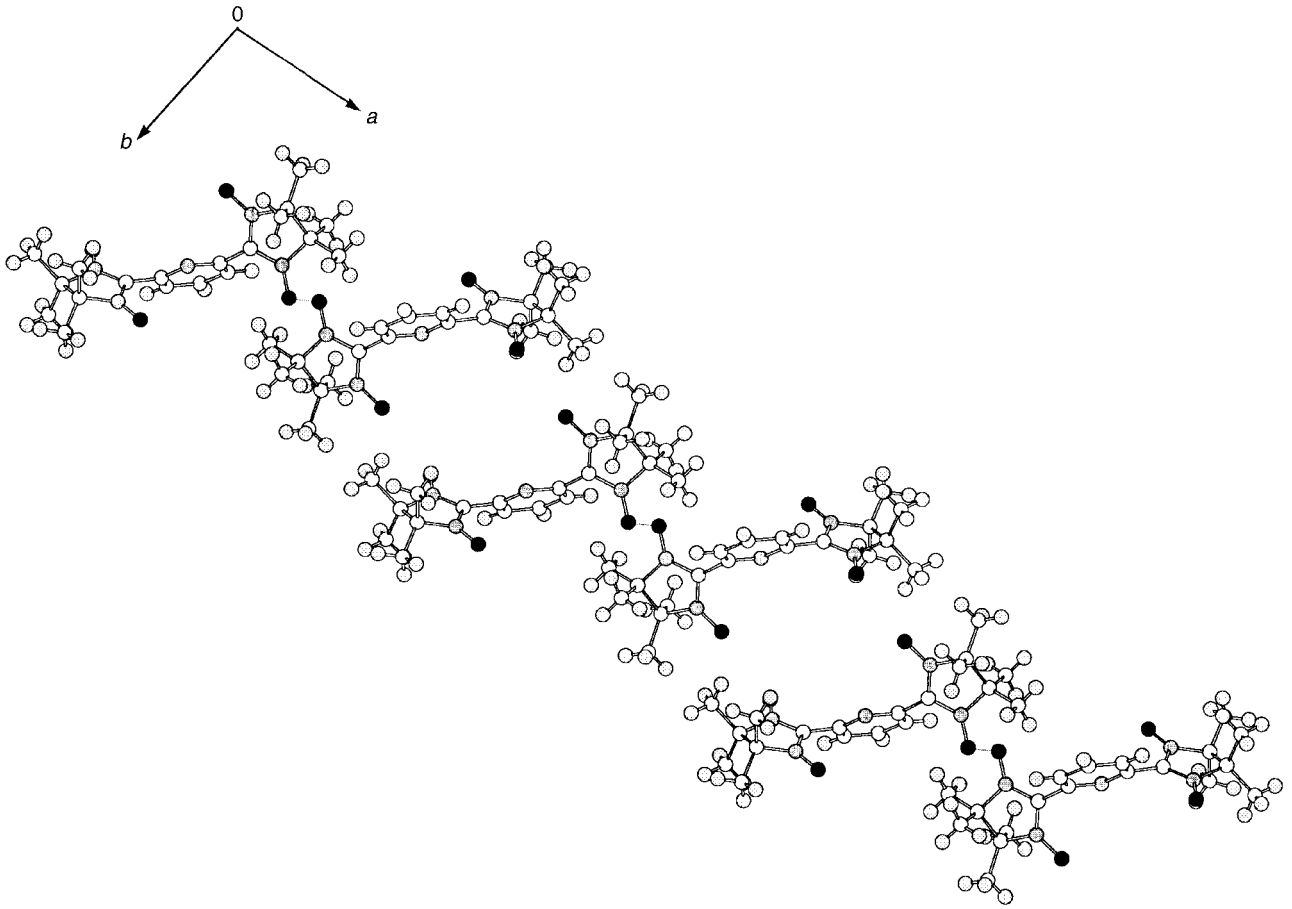

Fig. 5 Projection onto the *ab* plane of the crystal packing of compound **1c** showing the dimers running along the *a* direction.

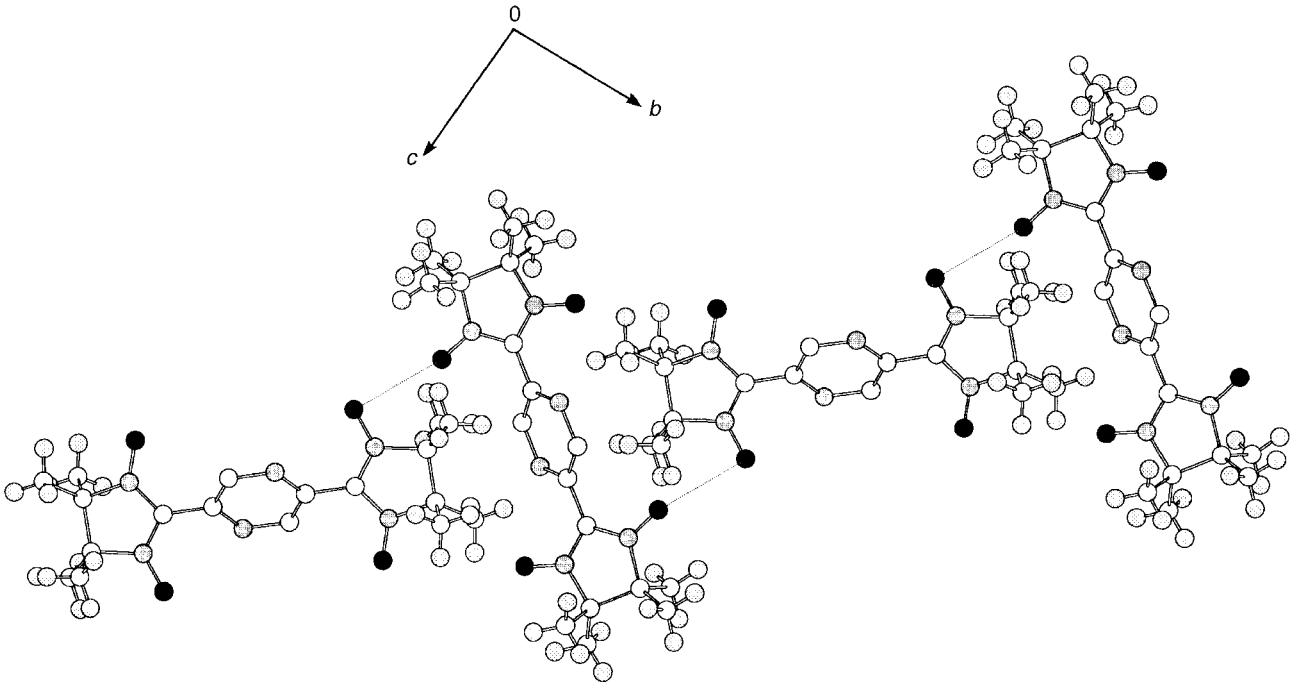

Fig. 6 Projection onto the *bc* plane of the crystal packing of compound **2c**.

6c and **7c** [displaying one nitrogen atom in an *ortho* position relative to the radical attachment point] are reduced to five lines as the temperature is lowered. These five lines are reminiscent of the coupling observed between two ^{14}N nuclei and a single unpaired electron. The ^{14}N coupling constant measured from the limiting five-line EPR spectra ranges from 7.5 to 7.6 G.

The spectral shapes and changes observed upon cooling these samples, see Fig. 9, are probably the result of an exchange broadening mechanism determined by a dynamic intramolecular process.[30] Most likely, this process corresponds to the out of phase internal rotation of the two radical moieties, which is able to modulate the exchange interaction *J*. It seems that in solution the biradical may exist in two or more confor-

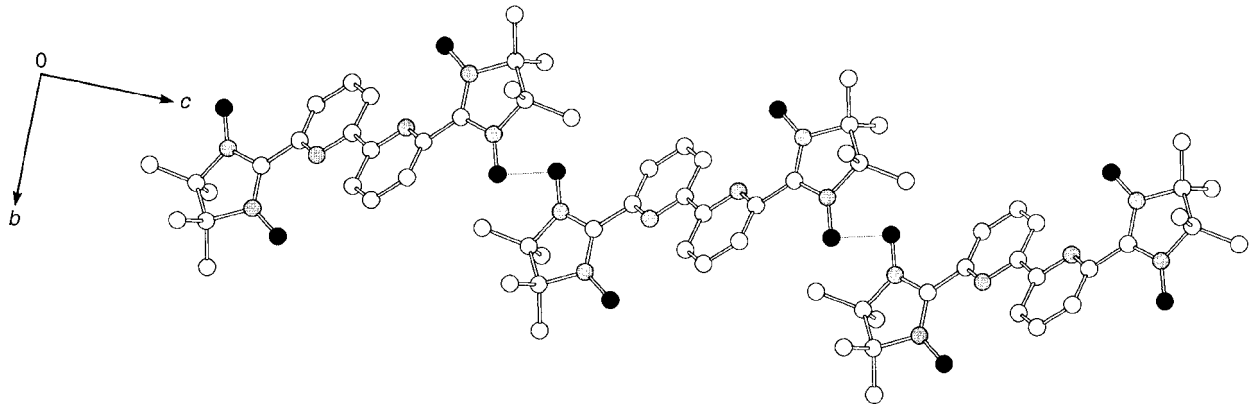

Fig. 7 Projection onto the *bc* plane of the crystal packing of compound **3c** showing the chains running along the *c* direction.

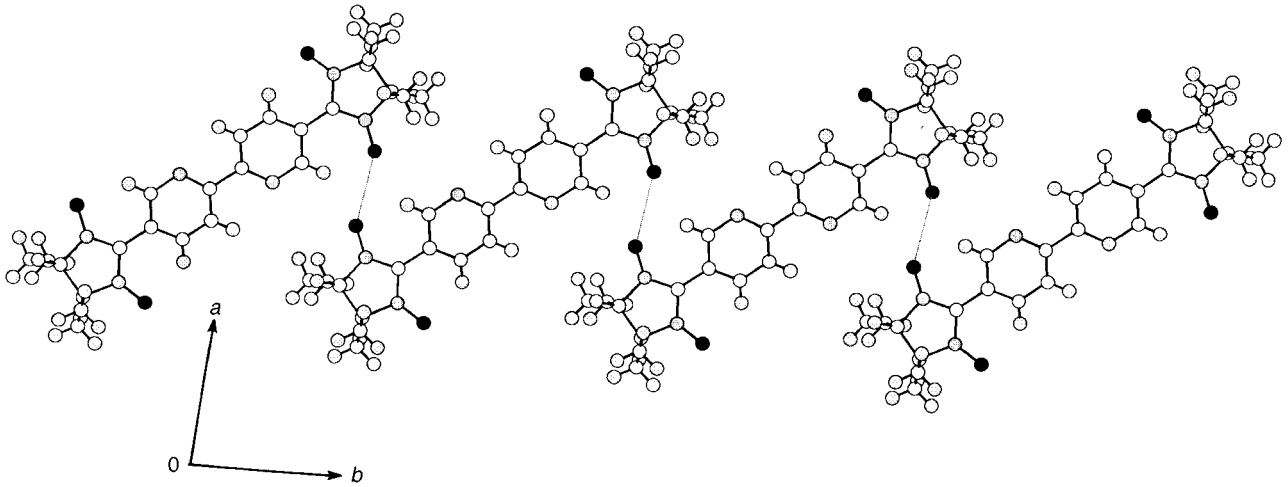

Fig. 8 Projection onto the *ab* plane of the crystal packing of compound **4c** showing the chains running along the *b* direction.

mations and these are characterized by different J values. At room temperature interconversion between these conformations is obviously fast on the EPR timescale, but slow at lower temperatures.

An attempt was made to observe the ($\Delta M_S = 2$) transition in these compounds by decreasing the temperature to 77 K. Only broadened EPR spectra due to anisotropy of the g tensor and nitrogen hyperfine tensor[31] were observed at this temperature.

The variable temperature EPR spectra of compounds **1c** and **4c** shown in Figs. 9 and 10 are representative of the effect of temperature on the exchange interactions in these compounds. These studies clearly reveal that the compounds functionalized in the *ortho* position relative to nitrogen (**1c**,

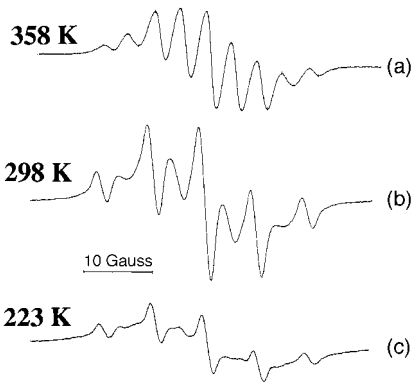

Fig. 9 X-Band EPR spectra of compound **1c** in dichloromethane at different temperatures.

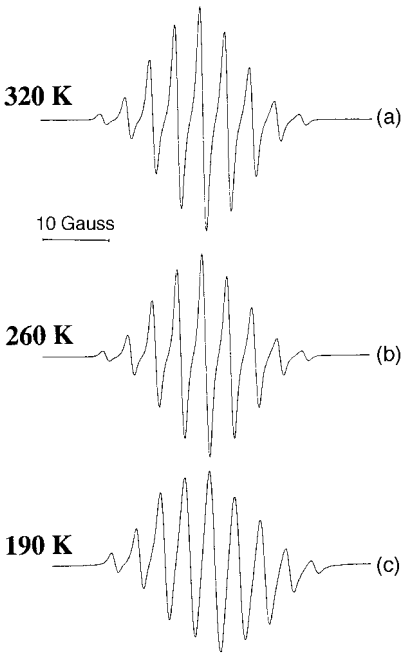

Fig. 10 X-Band EPR spectra of compound **4c** in dichloromethane at different temperatures.

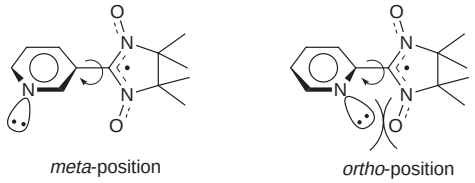

Scheme 2

2c, **3c**, **6c** and **7c**) exhibit a more restricted internal rotation process, perhaps due to the presence of the nitrogen lone pair. An interaction between the radical center and this lone pair could twist the nitroxide group out of planarity relative to the pyridine ring and slow down the free rotation (Scheme 2). In strong contrast, when the pyridine rings are functionalized in the *meta* positions such as in **4c** the stereoelectronic constraints are considerably attenuated and free rotation remains fast even at the lowest attainable temperatures. X-Ray diffraction analysis (see above) corroborates the fact that the tilt angle in **4c** is significantly less when compared to those of compounds **1c**, **2c** and **3c**.

Magnetic properties

The thermal variation of the molar magnetic susceptibility χ of microcrystalline samples has been measured down to 2 K with a SQUID susceptometer for most of the biradicals. The results are displayed in the form of χT *vs.* T or $1/\chi$ *vs.* T plots in Figs. 11 and 12, where T is the absolute temperature and χ the molar susceptibility. The χT values measured at 300 K for all biradicals lie in the 0.70 to 0.77 emu K mol^{-1} range, which corresponds almost exactly to the 0.75 emu K mol^{-1} value calculated for the spin only equation for two isolated $S=1/2$ or degenerate singlet–triplet systems. For the bipyridine, phenanthroline or pyridazine based radicals (**3c**, **4c**, **6c** and **7c**), as the temperature was lowered from 200 K the χT values decreased gradually until a sharp decrease was observed below 30 K, corresponding to antiferromagnetic coupling (Fig. 11). This coupling might occur either through the oligopyridine bridge (through-bond or intramolecular) or between the radicals of neighboring molecules (through-space or intermolecular). The intramolecular through-space process is excluded due to the large distance between the NN radicals

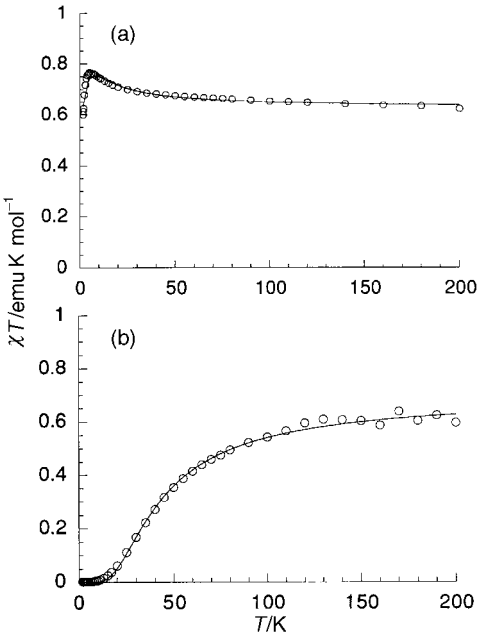

Fig. 12 Temperature dependence of the product of the magnetic susceptibility with temperature, χT *vs.* T, for compound **1c** (a) and for **2c** (b). The solid line represents the best-fit calculated values.

(*e.g.* >10 Å in **4c**). X-Ray diffraction analysis for **3c** and **4c** is suggestive of some intermolecular spin pairing and, in order to confirm this, we have measured the magnetic susceptibility of biradicals in frozen solution. The χT products were almost constant over the entire temperature range, thereby ruling out the intramolecular coupling pathway.

For all four biradicals the decrease of the χT product in the low temperature regime is due to weak intermolecular antiferromagnetic interactions between neighboring radicals. The strength of these interactions depends on the distance and relative orientation of the radicals.[29,32,33] Despite the larger O···O′ distance found for **3c** compared to **4c** (3.70 Å *versus* 3.01 Å), a significantly larger magnetic coupling constant is found for **3c** *versus* **4c**. This is due to a more appropriate geometry for π-orbital overlap of the radical centers in **3c** *versus* **4c** (O–N···O′ is 84 and 22°, respectively). The exper-

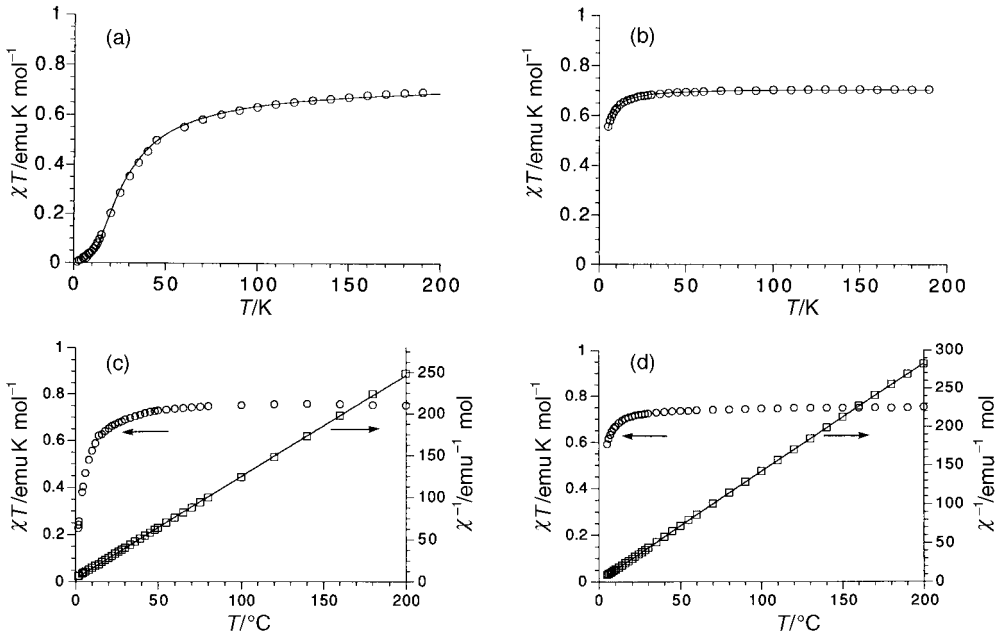

Fig. 11 Temperature dependence of the product of the magnetic susceptibility with temperature, χT *vs.* T, for compounds **3c** (a) and **4c** (b) and of the reciprocal susceptibility, $1/\chi$ *vs.* T and χT *vs.* T for **6c** (c) and for **7c** (d). The solid line represents the best-fit calculated values.

imental data were fitted by a Bleaney–Bowers expression[34] for an isolated two spins 1/2 model where the magnetic exchange coupling constant J corresponds to a Hamiltonian of the form $H=-2JS_1S_2$. Here a singlet–triplet splitting of $J/k_B=-24$ and -1.9 K was found for **3c** and **4c**, respectively with $g=2$ [Fig. 11(a) and 11(b)]. For compounds **6c** and **7c** the reciprocal susceptibility follows a Curie–Weiss law with $\theta=-3.5$ and -1.3 K, respectively [Fig. 11(c) and 11(d)], while intermolecular antiferromagnetic couplings are effective at temperatures lower than 30 K.

The most interesting results were obtained for the pyridine based biradicals **1c** and **2c** (Fig. 12). For **1c** an increase of the χT product is observed down to 100 K with a maximum value of 0.77 emu K mol^{-1}, then a decrease at lower temperature due to weak antiferromagnetic interactions. This temperature dependence of the $\chi_{mol}T$ values was analysed with the Bleaney–Bowers law for the magnetic susceptibility for a dimer but modified by including a mean-field approximation estimated by θ. This is considered to describe the average intermolecular interaction present in the crystal packing.[32]

The best parameters from a least-squares fit were $J/k_B=+9.4$ K and $\theta=-0.3$ K with $g=2$. The fact that the χT increase remains present when compound **1c** (3% in weight) is dispersed in a polystyrene matrix strongly suggests that the ferromagnetic interactions are effective through the conjugated π bonds of the pyridine ring. No intermolecular interactions are detected in the doped polystyrene film. Careful analysis of the crystal structure reveals that intermolecular contacts between two adjacent radicals are present (O1···O1′ 3.13 Å) but that the relative orientation of these radicals ($\alpha=52°$) does not favour efficient orbital overlap.[29] Therefore only a weak antiferromagnetic interaction is expected and indeed observed experimentally [Fig. 12(a)]. Nothing in the crystal packing of **1c** would suggest a favourable orientation of the π orbitals leading to a ferromagnetic behaviour. When **1c** crystallized in a different space group ($P2_1/a$) the peculiar magnetic behavior was interpreted in term of a four-spin system associated with a combined effect of ferro- and antiferro-magnetic coupling.[35] The through-bond or through-space character of these magnetic coupling interactions was, however, not specifically addressed.[35] Such a mathematical model was not needed here to parametrize the temperature dependence of the magnetic susceptibility of compound **1c**.

The magnetic behavior of compound **2c** strongly contrasts with the one observed for **1c**. As the temperature was lowered the $\chi_{mol}T$ values decreased continuously to nearly zero as shown in Fig. 12(b). The Bleaney–Bowers expression was applied to the $\chi_{mol}T$ *versus* T plot without a Weiss field since the crystal structure of **2c** from the X-ray analysis shows that the molecules are quasi-isolated with the shortest O···O′ distances being as long as 5.77 Å. The Bleaney–Bowers expression[34] was applied to the experimental data by means of a least-squares method to give the best fit parameter $J/k_B=-39$ K. Most of the antiferromagnetic interaction remains when **2c** is dispersed in a polystyrene matrix which strongly suggests that the antiferromagnetic interactions are also intramolecular and propagated through the π system of the pyridine ring.

The results obtained for compounds **1c** and **2c** confirm the key role played by the spin polarization in a single ring π conjugated system on the sign of the exchange coupling.[36] It also highlights the tremendous attenuation of the spin polarization effect when a second pyridine ring is present. Indeed, no significant intramolecular interaction could be found in the oligopyridine based radicals **3c** to **6c**.

Electrochemical results

The electrochemistry of these new oligopyridine based nitronyl nitroxides is very interesting. The two essentially independent

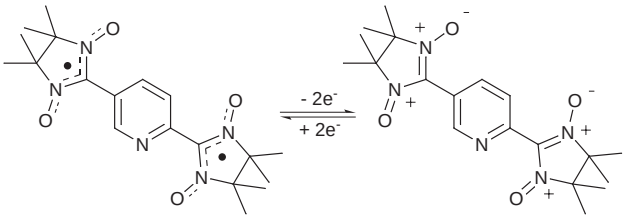

Scheme 3

nitroxide groups are simultaneously oxidized in a two-electron quasi-reversible process to the nitrosonium dications. The cyclic voltammograms for such two-electron processes indicate single apparent potentials for the reduction and oxidation of the two nitroxide groups in most of the compounds we studied. However, it is important to remember that there exists a statistical difference[37] between such potentials. Nitrosonium cations resulting from electrochemical oxidation of some cyclic nitroxides such as 2,2′6,6′-tetramethylpiperidine 1-oxyl (Tempo) have been reported by Tamura[38] and Malinski *et al.*[39] Scheme 3 illustrates the formation of such dications from the bis(nitronyl nitroxide) compounds. The cyclic voltammograms for the electrochemical conversion of these compounds into the nitrosonium dications is illustrated by those of compound **6c** shown in Fig. 13. The corresponding cyclic voltammograms obtained at different scan rates are shown in Fig. 13(b). The large separation between the anodic and cathodic peak potentials (see Table 3) and the dependency of these potentials on scan rate are typical of quasi-reversible systems.

The bis(nitronyl nitroxide) compounds are all irreversibly reduced. Fig. 14 represents typical cyclic voltammograms exhibited by these compounds. We believe the two independent nitroxide units in these compounds are simultaneously reduced to the anions which subsequently react with traces of water present in the solvent to form the dihydroxylamines. Precedence for this observation has been reported by Malinsk *et al.*[39] and Serve.[40] Thus the electrochemical–chemical mechanistic pathway for the reduction of these compounds can be written using the structure of **2c** as an example (Scheme 4).

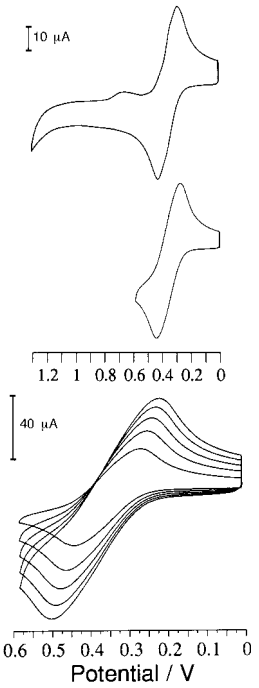

Fig. 13 Cyclic voltammograms for compound **6c**, in dichloromethane, at a scan rate of 100 mV s^{-1} over the potential range 0–1.3 V (a) and at scan rates of 500, 400, 300, 200 and 100 mV s^{-1} over the potential range 0–0.6 V (b).

Table 3 Cathodic and anodic peak potentials (V) *vs.* Ag/Ag^+ for the bis(nitronyl nitroxide) compounds[a]

Compound	Reduction	Oxidation	ΔE_p/V
1c	$E_{pc} = 1.76$	$E_{pa} = 0.46$	
	$E_{pa} = NO$	$E_{pc} = 0.27$	0.19
2c	$E_{pc} = 1.79$	$E_{pa} = 0.46$	
	$E_{pa} = NO$	$E_{pc} = 0.24$	0.22
3c	$E_{pc} = 1.60$	$E_{pa} = 0.36$	
	$E_{pa} = NO$	$E_{pc} = 0.26$	0.10
4c	$E_{pc} = 1.42$	$E_{pa} = 0.43$	
	$E_{pa} = NO$	$E_{pc} = NO$	
6c	$E_{pc} = 1.60$	$E_{pa} = 0.42$	
	$E_{pa} = NO$	$E_{pc} = 0.28$	0.14
7c	$E_{pc} = 1.72$	$E_{pa} = 0.43$	
	$E_{pa} = NO$	$E_{pc} = 0.32$	0.11

[a]In 0.1 M NBu_4ClO_4–dichloromethane solution at a glassy carbon electrode; NO = Not observed; E_{pc} = cathodic peak potential; E_{pa} = anodic peak potential.

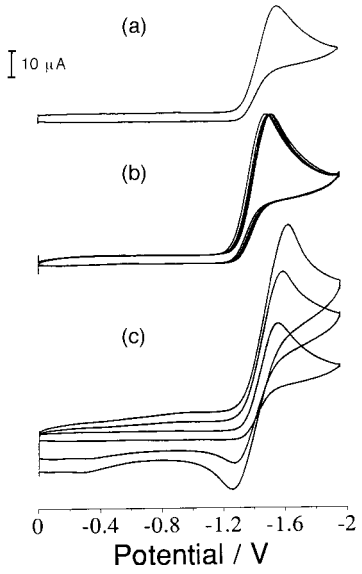

Fig. 14 Cyclic voltammograms for the reduction of compound **3c** in dichloromethane (a) at a scan rate of 100 mV s^{-1}, (b) multiple scan at a scan rate of 100 mV s^{-1} and (c) variable scan at scan rates of 1000, 500 and 100 mV s^{-1}.

The potentials for oxidation and reduction during the anodic and cathodic scans as well as the peak-to-peak separation (ΔE_p) for oxidation of these compounds are gathered in Table 3.

The Cu(II) and Ni(II) complexes **8–11** possess several electroactive centers. Unlike the 'free' ligands (**3c** and **6c**), the redox chemistry of these complexes is expected to be influenced by the presence of the electropositive metal ions. Indeed, upon reduction of the Ni(II) complexes of **3c** and **6c** two separate quasi-reversible redox processes were observed (Fig. 15). The voltammograms suggest that the two nitroxide groups in these complexes are equivalent and independent of one another. They are therefore simultaneously reduced in a two-electron

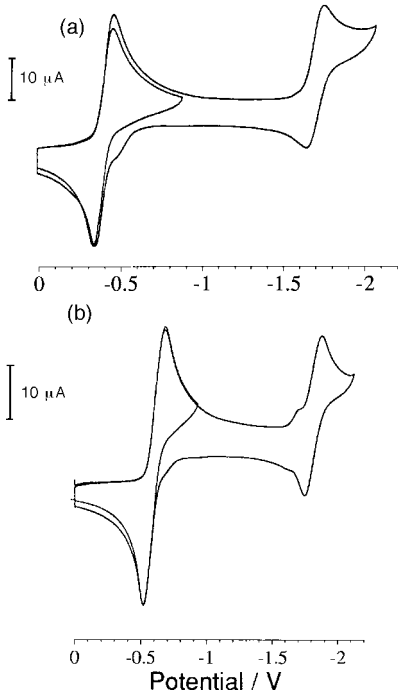

Fig. 15 Cyclic voltammograms for the reduction, in dichloromethane, at a scan rate of 100 mV s^{-1} of (a) nickel(II) complex **9** and (b) nickel(II) complex **11**.

quasi-reversible process to the hydroxylamine anions. Thus the first redox couple represents the reduction of the nitroxide groups to the hydroxylamine anions which are subsequently converted into the starting complexes upon reversal of the scan direction. The large potential shift (*ca.* 1.20 V *versus* the 'uncomplexed' ligand) is a consequence of strong stabilization of these anions by complexation to the dicationic metal center. The absence of a chemical reaction following the initial electrochemical step is attributed to additional stabilization provided by the metal ions. This is also reflected in the reduction potentials of the nitroxide groups in these complexes compared to those in **3c** and **6c**. The second redox couple in the voltammograms shown in Fig. 15 represents the monoelectronic reduction of bipyridine and phenanthroline groups to the respective anions which are reoxidized quasi-reversibly upon reversal of the scan direction. Such ligand based reductions have also been reported by Bartak[40] and Bard *et al.*[41]

Like the Ni(II) complexes, the Cu(II) complexes of **3c** and **6c** exhibit two main redox processes upon reduction. Fig. 16 represents a typical cathodic voltammetric response of the Cu(II) complex of **3c**. The first redox signal consists of two closely spaced redox couples which are better resolved in the Osteryoung square wave voltammograms. The observation of these two closely spaced reduction waves for each of these complexes attests to the fact that the two nitroxide groups in each are electronically coupled and are therefore sequentially reduced at different potentials. The reduction wave centered

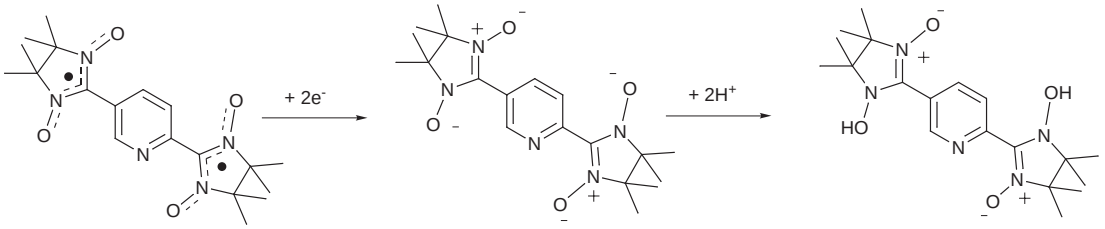

Scheme 4

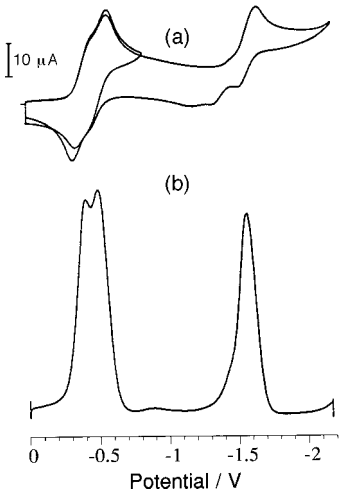

Fig. 16 Cyclic voltammograms for the reduction of copper(II) complex **8**, in dichloromethane, (a) at a scan rate of 100 mV s^{-1} and (b) Osteryoung square wave voltammogram at a frequency of 15 Hz, square wave amplitude of 25 mV and a potential step of 4 mV.

at −1.67 V for each of these complexes is due to reduction of the bipyridine and phenanthroline moieties, respectively. The Ni(II) and Cu(II) complexes of **3c** and **6c** also formed nitrosonium dications upon oxidation *via* a two-electron quasi-reversible process. These dications are formed at more positive potentials than those of the ligands. The dications formed upon oxidation of the Cu(II) complexes are not stable on the cyclic voltammetric timescale. Some decomposition products are evident in the cathodic voltammetric response corresponding to the reduction of the nitrosonium dications to the nitroxides. Although most of the bis(nitronyl nitroxide) oxidation or redox products are stable on the cyclic voltammetric timescale, they are not stable on the coulometric timescale. In an effort to probe the fate of the oxidized species, we subjected the bis(nitronyl nitroxide) compounds to exhaustive electrolysis. Electrolytic oxidation followed by EPR examination of the products revealed that the diamagnetic nitrosonium cations[22,43,44] had decomposed to unknown paramagnetic species. The EPR spectra of such species exhibit seven main lines and some minor splittings. The seven lines have a pattern similar to those of imino nitroxides.[15,45] This suggests that the nitrosonium dications formed upon electrolytic oxidation decompose to products which contain at least an imino nitroxide. The mechanism by which this transformation occurs is not clear to us at this moment. Since the bis(nitronyl nitroxide) compounds are irreversibly reduced, no attempt was made to subject these compounds to electrolytic reduction. However, the Cu(II) and Ni(II) complexes of **3c** and **6c** were subjected to coulometric reduction. The EPR spectra before and after coulometry of these complexes are entirely different. Such spectra recorded after coulometric reduction of the Cu(II) complexes of **3c** and **6c** closely resemble those of the 'free' ligands **3c** and **6c**. Evidently, coulometric reduction of these complexes is accompanied by formation of the 'free' ligands. Similar observations have been reported for $[Ru(bpy)_3]^{2+}$,[42] Co(II)/bpy,[46] Mn(II)/bpy,[47] and $[Fe(bpy)_3]^{2+}$ complexes in acetonitrile.[48]

Nickel complex **13** shows four successive redox processes upon reduction, the first two being dielectronic while the last two are monoelectronic. The cyclic voltammograms for reduction of **13** are shown in Fig. 17(a) with the corresponding square wave voltammogram in Fig. 17(b). The square wave voltammogram suggests that two sets of equivalent nitroxide groups are present in **13**. The third and fourth redox processes correspond to successive reduction of the two bridging pyridine groups which are non-equivalent. The peak potentials for oxidation and reduction of these complexes are gathered in

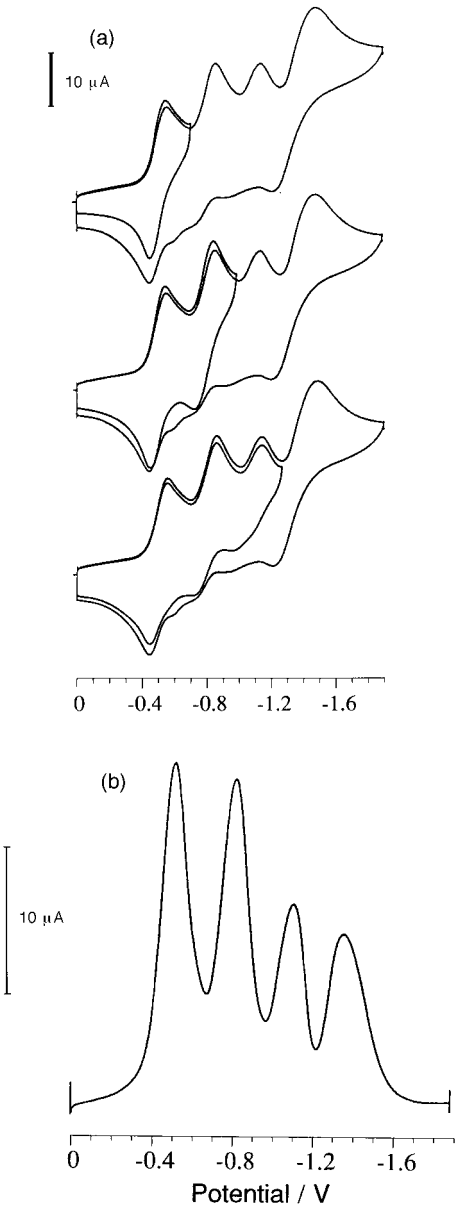

Fig. 17 Cyclic voltammograms for the reduction of nickel(II) complex **13**, in dichloromethane, at a scan rate of 100 mV s^{-1}, demonstrating the effect of reversing scan direction (a) after the first wave (top), after the second wave (middle), and after the third wave (bottom); (b) Osteryoung square wave voltammogram at a frequency of 15 Hz, square wave amplitude of 25 mV and a potential step of 4 mV.

Table 4. Oxidation of both nitroxide groups to the corresponding nitrosonium cations is more difficult compared to the 'free' ligands by *ca.* 0.8 V owing to the presence of the divalent metal center.

Conclusion

This study has revealed some interesting observations about the physical properties of bis(nitronyl nitroxide) oligopyridinic compounds. Magnetic measurements and their interpretation reveal that the through-bond interaction between the two radical centers is only present in the pyridine based biradicals. In all other cases weak through-space antiferromagnetic interactions are predominant. EPR studies showed that the intramolecular spin–spin interactions in these compounds are modulated by temperature. At cryogenic temperatures, the EPR spectra of these compounds are dominated by anisotropies in nitrogen hyperfine coupling and g tensors. The observed anisotropic broadening of the EPR spectra of these

Table 4 Cathodic and anodic peak potentials (V) *vs.* Ag/Ag^+ for complexes **8** to **11**[a]

Complex	Oxidation	Reduction		
		I	II	III
8	$E_{pa}=1.12$	$E_{pc}=0.45$	$E_{pc}=0.59$	$E_{pc}=1.67$
	$E_{pc}=0.97$	$E_{pa}=0.34$	$E_{pa}=0.49$	$E_{pa}=1.54$
10	$E_{pa}=1.10$	$E_{pc}=0.46$	$E_{pc}=0.57$	$E_{pc}=1.67$
	$E_{pc}=0.95$	$E_{pa}=0.35$	$E_{pc}=0.47$	$E_{pa}=1.57$
9	$E_{pa}=1.06$	$E_{pc}=0.48$	$E_{pc}=1.78$	
	$E_{pc}=0.90$	$E_{pa}=0.35$	$E_{pa}=1.67$	
11	$E_{pa}=1.01$	$E_{pc}=0.71$	$E_{pc}=1.92$	
	$E_{pc}=0.86$	$E_{pa}=0.52$	$E_{pa}=1.80$	
13	$E_{pa}=1.03$	$E_{pc}=0.56$	$E_{pc}=0.86$	

[a]In 0.1 M NB_4ClO_4–dichloromethane solution at a glassy carbon electrode (redox couples referred to as first (I), second (II), and third (III)); E_{pc} = cathodic peak potential; E_{pa} = anodic peak potential.

Table 5 Crystallographic data for compounds **2c** and **4c**

	2c	**4c**
Empirical formula	$C_{19}H_{27}N_5O_4$	$C_{24}H_{30}N_6O_4$
Formula weight	389.5	466.5
Crystal color	Violet	Green
Crystal system	Monoclinic	Monoclinic
Space group	$P2_1/c$	$P2_1/n$
a/Å	6.192(2)	17.216(5)
b/Å	11.794(3)	10.832(3)
c/Å	13.513(4)	6.247(2)
β/°	93.74(2)	95.71
V/Å^3	984.7	1159.2
Z	2	2
D/g cm^{-3}	1.312	1.337
Radiation	Cu-Kα graphite monochromated	Cu-Kα graphite monochromated
No. observations ($I>3\sigma I$)	966	1025
R/R_w'	0.045/0.078	0.040/0.060

molecules is one of the reasons that nitroxides have found useful applications in spin labelling, their sole purpose being to report changes in the motion and/or environment of the larger molecule to which they are attached. The biradicals examined in this study could be useful in probing the environment of complex systems such as vesicles.

Electrochemical reduction of the bis(nitronyl nitroxide) compounds is complicated by chemical reactions. Oxidation resulted in formation of the nitrosonium dications. The corresponding metal complexes exhibit some interesting electrochemical properties. Upon oxidation they also formed the nitrosonium dications but at more positive potentials than those formed by the bis(nitronyl nitroxides). Reduction of these complexes resulted in simultaneous reduction of the nitroxide groups in addition to reduction of the spacer units.

Experimental

EPR Spectroscopy

X-Band EPR spectra were obtained on a Bruker ER-200D spectrometer equipped with a variable-temperature accessory. A 100 kHz magnetic field modulation was used. The solution samples (≈1 mM) were degassed by three freeze–pump–thaw cycles and sealed *in vacuo*. Spectra at 77 K were recorded using a Dewar insert. All EPR experiments were conducted under vacuum conditions. The solvent dichloromethane (Aldrich) was distilled over P_2O_5 under vacuum conditions.

Electrochemistry

Electrochemical experiments were performed using Bioanalytical Systems 100 and 100B analysers, equipped with *IR* compensation. A Houston DMP-40 plotter and Hewlett-Packard color plotter were used to record the voltammograms. The dichloromethane used in the electrochemical studies was also distilled over P_2O_5 under vacuum conditions. Electroactive samples were present at a concentration of ≈1 mM. The reference electrode consisted of a silver wire immersed in 0.1 M *n*-tetrabutylammonium perchlorate solution containing 10 mM $AgNO_3$ in dichloromethane–acetonitrile (9:1). The supporting electrolyte, *n*-tetrabutylammonium perchlorate (Fluka), was recrystallized from ethyl acetate twice and dried at 80 °C for ≈15 h in a vacuum oven. Glassy carbon was used as the working electrode for electrochemical studies. It was polished with a diamond paste (METADI) of particle sizes 3 and 0.25 μm. The counter electrode was a platinum wire. Electrolytic reductions/oxidations were carried out at a platinum mesh surface with a silver wire as pseudoreference.

X-Ray crystallographic analysis

Single crystals were isolated from a cluster of crystals and mounted on a rotation-free goniometer head. Systematic searches in reciprocal space using a Philips PW1100/16 automatic diffractometer with Cu-Kα graphite monochromated radiation showed that crystals of **1c**, **2c** and **4c** belong to the monoclinic space group ($P2_1/c$ for the first two and $P2_1/n$ for the last). Quantitative data were obtained at −100 °C for all compounds. Selected experimental parameters are given in Table 5. The resulting data sets were transferred to a DEC Alpha work station and subsequent calculations made with the Nonius OpenMoleN package.[49] Three standard reflections measured every hour during the entire data collections period showed no significant trend. The raw data were converted into intensities and corrected for Lorentz polarization factors.

The structures were solved using direct methods. After refinement of the heavy atoms, Fourier-difference maps revealed maxima of residual electronic density close to the positions expected for hydrogen atoms; they were introduced into structure-factor calculations by their computed coordinates (C–H 0.95 Å) and isotropic thermal parameters such as $B(H)=1.3\ B_{eq}(C)$ Å^2 but not refined (full matrix least-squares refinements). Final difference maps revealed no significant maxima. The scattering factor coefficients and anomalous dispersion coefficients, respectively, were taken from ref. 50(*a*) and 50(*b*).

Full crystallographic details, excluding structure factors, have been deposited at the Cambridge Crystallographic Data Centre (CCDC). See Information for Authors, 1999, Issue 1. Any request to the CCDC for this material should quote the full literature citation and the reference number 1145/145. See http://www.rsc.org/suppdata/jm/1999/1435 for crystallographic files in .cif format.

Other instrumentations

Mps are uncorrected; Büchi-535 capillary melting point apparatus in open ended capillaries. UV/VIS spectra: Shimatzu UV-260 or Perkin-Elmer Lambda 5 spectrophotometer. FT-IR spectra: Bruker IFS 25 spectrometer; KBr pellets. NMR spectra: at R.T. unless otherwise noted; Bruker-SY-200 or AC-200 (200.1 (^{1}H) or 50.3 MHz (^{13}C); δ(H) in ppm relative to the solvent $CDCl_3$ (7.25), d_6-DMSO (2.50), d_5-pyridine (8.70, 7.58, 7.20), CD_3OD (δ 3.35); δ(C) in ppm relative to the solvent $CDCl_3$ (77.0), d_5-pyridine (δ 124–150), CD_3OD (δ 49.3). MS: fast-atom bombardment (FAB, positive mode ZAB-HF-VG-Analytical apparatus in a *m*-nitrobenzyl alcohol matrix unless otherwise specified.

Materials

NBS (Fluka), azobisisobutyronitrile (AIBN) (Janssen), SiO_2 (Merck), alumina (Merck), sodium periodate (Janssen), silver oxide (Strem), copper perchlorate hexahydrate (Janssen), nickel perchlorate hexahydrate (Fluka).

Preparations

2,6-Bis(1,3-dihydroxy-4,4,5,5-tetramethylimidazolin-2-yl)-pyridine 1b. A mixture of 2,3-bis(hydroxyamino)-2,3-dimethylbutane (0.56 g, 3.8 mmol) and 0.25 g of 2,6-diformylpyridine **1a** (1.85 mmol) in 50 mL of methanol was stirred at room temperature for 3 d. The precipitate was filtered off to obtain compound **1b** in 52% yield. ^{1}H NMR (d_6-DMSO): δ 7.72 (s, 4 H, OH), 7.54 (s, 2H, $H_{3,5}$ pyridine), 7.50 (s, 1H, H_4 pyridine), 4.67 (s, 2H, CH imidazoline), 1.08 (s, 24H, CH_3) ^{13}C-{^{1}H} NMR (d_5-pyridine): δ 161.7 (C_{quat} pyridine), 121.3, 92.5 (CH imidazoline), 67.4 (C_{quat} imidazoline), 24.6 (CH_3), 18.3 (CH_3) IR (KBr): 3405s (ν_{OH}), 2982 m, 2932 m, 1596w, 1577w, 1460s, 1371s, 1161s cm^{-1}. FAB$^+$ m/z 396, [M+H]$^+$.

2,6-Bis(4,4,5,5-tetramethylimidazoline 3-oxide 1-oxy 2-yl)-pyridine 1c. To a suspension of compound **1b** (0.155 g, 0.37 mmol) in dichloromethane (50 mL) was added an aqueous solution (50 mL) of sodium periodate (0.15 g, 0.73 mmol). The biphasic mixture was stirred for one hour. The product was extracted with dichloromethane and the organic layers were dried over magnesium sulfate. After chromatography (alumina, $CH_3CO_2C_2H_5$–MeOH 95:5, R_f=0.5), and recrystallization of the blue fractions by slow evaporation from a CH_2Cl_2–hexane solution, deep blue crystals (0.094 g, 64%) were obtained, mp 226 °C (decomp.). IR (KBr): 2986w, 1586w, 1453 m, 1412s, 1368s (ν_{NO}), 1187 m, 1133 m cm^{-1}. UV-Vis (CH_2Cl_2): λ/nm (ε/M^{-1} cm^{-1}) 570 (720) (n→π*, NO), 369 (25 000), 273 (18 300) (π→π*, pyridine), 233 (14 200). FAB$^+$ m/z 390, [M+H]$^+$; 375 [M−O+2H], 359 [M−2O+2H], 344 [M−3O+3H], 328 [M−4O+3H] (Calc. for $C_{19}H_{27}N_5O_4$: C, 58.60; H, 6.99; N, 17.98. Found: C, 58.49, H, 6.91, N, 17.92%).

2,5-Bis(4,4,5,5-tetramethylimidazoline 3-oxide 1-oxy 2-yl)-pyridine 2c. To a solution of 2,5-diformylpyridine **2a** (0.25 g, 1.85 mmol) in methanol (50 mL) was added 2,3-bis(hydroxyamino)-2,3-dimethylbutane (0.55 g, 3.7 mmol). The mixture was stirred for 3 d and the solvent then removed under vacuum. The resulting solid was oxidized in dichloromethane with silver oxide (0.4 g) for 2 h. The filtrate obtained after removing the solid particles was chromatographed (Al_2O_3, ethyl acetate–MeOH 95:5, R_f=0.82), and a recrystallization of the blue fractions (CH_2Cl_2–hexane) gave deep blue crystals (0.023 g, 3%). IR (KBr): 2983 m, 1591w, 1462 m, 1414s, 1351s (ν_{NO}), 1293 m, 1168 m, 1137s cm^{-1}; UV-Vis (CH_2Cl_2): λ/nm (ε/M^{-1} cm^{-1}) 585 (550) (n→π*, NO), 376 (17 000), 317 (20 000), 284 (20 100) (π→π*, pyridine). FAB$^+$ m/z 390, [M+H]$^+$ (Calc. for $C_{19}H_{27}N_5O_4$: C, 58.60; H, 6.99; N, 17.98. Found: C, 58.52, H, 6.91, N, 17.90%).

6,6′-Bis(1,3-dihydroxy-4,4,5,5-tetramethylimidazolin-2-yl)-2,2′-bipyridine 3b. A solution of 2,3-bis(hydroxyamino)-2,3-dimethylbutane (0.35 g, 2.3 mmol) and 0.25 g of 6,6′-diformyl-2,2′-bipyridine **3a** (1.3 mmol) in 60 mL of methanol was stirred at room temperature for 3 d. Then the precipitate was removed to obtain a yield 72% of the adduct **3b**, mp 245 °C (decomp.). ^{1}H NMR (d_6-DMSO): δ 8.32 (d, 2 H, ^3J=7.5, $H^{3,3'}$ bpy), 7.95 (m, 2H), 7.81 (s, 4H, OH), 7.63 (d, 2H, J=7.6 Hz, $H^{5,5'}$ bpy), 4.75 (s, 2H, CH imidazoline), 1.13 (s, 12H, CH_3), 1.11 (s, 12H, CH_3). ^{13}C-{^{1}H} NMR (d_5-pyridine): δ 137.8, 136.7, 122.3, 121.7, 120.1, 92.8, 67.6, 28.6, 25.9, 24.6, 23.9, 19.5, 18.2. IR (KBr): 3254s (ν_{OH}), 2975 m, 2828 m, 1577 m, 1444s, 1371 m, 1148s cm^{-1}. FAB$^+$ m/z 473 [M+H]$^+$.

6,6′-Bis(4,4,5,5-tetramethylimidazoline 3-oxide 1-oxy 2-yl)-2,2′-bipyridine 3c. To a suspension of compound **3b** (0.43 g, 0.9 mmol) in dichloromethane (50 mL) was added an aqueous solution (50 mL) of sodium periodate (0.49 g, 2.3 mmol). The biphasic mixture was stirred for one hour. The product was extracted with dichloromethane and the organic layers were dried over magnesium sulfate. Short column chromatography (alumina, $CH_3CO_2C_2H_5$–MeOH 95:5, R_f=0.65), and recrystallization of the blue fractions (CH_2Cl_2–hexane), gave deep blue crystals (0.3 g, 70%), mp 235 °C. IR (KBr): 2993 m, 1577 m, 1452s, 1411s, 1358s (ν_{NO}), 1181 m, 1140 m cm^{-1}. UV-Vis (CH_2Cl_2): λ/nm (ε/M^{-1} cm^{-1}) 575 (740) (n→π*, NO), 369 (24 500), 277 (25 600) (π→π*, bpy), 234 (27 100). FAB$^+$ m/z 467, [M+H]$^+$; 451 [M−O+H], 436 [M−2O+2H], 420 [M−30+2H] (Calc. for $C_{12}H_{15}N_3O_2$: C, 61.79; H, 6.48; N, 18.01. Found: C, 61.62, H, 6.42, N, 17.93%).

5,5′-Bis(1,3-dihydroxy-4,4,5,5-tetramethylimidazolin-2-yl)-2,2′-bipyridine 4b. A solution of 2,3-bis(hydroxyamino)-2,3-dimethylbutane (0.648 g, 4.6 mmol), and 0.45 g of compound **4a** (2.1 mmol) in 30 mL of methanol was stirred at room temperature for 3 d. Removal of the precipitate and concentration of the mother-liquors led to a second crop and an 85% yield of **4b**. ^{1}H NMR (d_6-DMSO): δ 8.70 (s, 2H, $H^{6,6'}$-bpy), 8.34 (d, 2H, ^3J=8.0, $H^{3,3'}$-bpy), 7.98 (d, 2H, ^3J=7.1 Hz, $H^{4,4'}$-bpy), 7.92 (s, 2H, OH exchange with D_2O), 7.60 (s, 2H, OH exchange with D_2O), 4.62 (s, 2H, CH imidazoline), 1.05 (m, 24H, CH_3). ^{13}C-{^{1}H} NMR (d_5-pyridine): δ 156.0, 140.1, 136.7, 135.9, 121.1, 89.5, 78.6, 67.4, 60.7, 28.8, 25.4, 25.1, 24.2, 24.0, 22.2, 19.4, 17.9, 15.2. IR (KBr): 3254s (ν_{OH}), 2979 m, 1595 m, 1467s, 1367s, 1151s cm^{-1}. FAB$^+$ m/z 473, [M+H]$^+$; 457 [M−O+H], 441 [M−2O+H].

5,5′-Bis(4,4,5,5-tetramethylimidazoline 3-oxide 1-oxy 2-yl)-2,2′-bipyridine 4c. To a suspension of compound **4b** (0.05 g, 0.1 mol) in dichloromethane (10 mL) was added an aqueous solution (10 mL) of sodium periodate (0.075 g, 0.3 mmol). The biphasic mixture was stirred for one hour. The product was extracted with dichloromethane and the organic layers were dried over magnesium sulfate. Short column chromatography (alumina, $CH_3CO_2C_2H_5$–MeOH 95:5, R_f=0.78), and a recrystallization of the green fractions (CH_2Cl_2–hexane), gave deep green crystals (0.025 g, 52%), mp >250 °C (decomp.). IR (KBr): 2975 m, 1592 m, 1453 m, 1420s, 1370 m, 1347s (ν_{NO}), 1135 m cm^{-1}. UV-Vis (CH_2Cl_2): λ/nm (ε/M^{-1} cm^{-1}) 607 (320) (n→π*, NO), 532 (350) (n→π*, NO), 318 (30 000), 256 (14 100), FAB$^+$: m/z 467, [M+H]$^+$; 452 [M−O+2H], 436 [M−2O+2H], 421 [M−3O+3H], (Calc. for $C_{12}H_{15}N_3O_2$: C, 61.79; H, 6.48; N, 18.01. Found: C, 61.50, H, 6.26; N, 17.73%).

4,4′-Bis(1,3-dihydroxy-4,4,5,5-tetramethylimidazolin-2-yl)-2,2′-bipyridine 5b. A solution of 2,3-bis(hydroxyamino)-2,3-dimethylbutane (0.367 g, 2.5 mmol), and 0.250 g of compound **5a** (1.2 mmol) in 30 mL of methanol were stirred at room temperature for 3 d. Removal of the precipitate gave 0.2 g (36%) of **5b**. ^{1}H NMR (d_6-DMSO): δ 8.70 (m, 4 H), 7.98 (br s, 2H), 7.66 (s, 2H, OH), 7.52 (s, 2H, OH), 4.60 (s, 2H, CH imidazoline), 1.05 (m, 24H, CH_3). ^{13}C-{^{1}H} NMR (d_5-pyridine): δ 153.4, 150.3, 149.1, 124.5, 123.9, 121.4, 90.7, 79.9, 67.6, 60.9, 28.6, 24.9, 22.3, 18.0, 15.4. IR (KBr): 3252s (ν_{OH}), 2981 m, 1594 m, 1465s, 1370 m, 1153s cm^{-1}. FAB$^+$ m/z 473 [M+H]$^+$; 457 [M−O+H].

2,9-Bis(4,4,5,5-tetramethylimidazoline 3-oxide 1-oxy 2-yl)-1,10-phenanthroline 6c. 2,9-Diformyl-1,10-phenanthroline **6a** (1 g, 4.2 mmol) was stirred in 100 mL of methanol with 2,3-bis(hydroxyamino)-2,3-dimethylbutane (1.25 g, 8.4 mmol) for three days. The solvent was removed under vacuum, and the resulting solid solubilized in dichloromethane (100 mL). An

aqueous solution of $NaIO_4$ (2.7 g, 12.6 mmol, in 50 mL water) was then added and stirred for 1 h. The organic layer was removed, washed with water, and dried over magnesium sulfate. After chromatography (alumina, ethyl acetate–methanol 95:5) a purple fraction was obtained. Recrystallization in a dichloromethane–hexane mixture, by slow evaporation of dichloromethane, gave deep purple crystals of **6c** (0.2 g, 10%). IR (KBr): 2979 m, 1553 m, 1470 m, 1425s, 1376s (ν_{NO}), 1166 m, 1146s cm^{-1}. UV-Vis (CH_2Cl_2): λ/nm ($\varepsilon/M^{-1}\,cm^{-1}$) 569 (607) (n→π*, NO), 392 (9400), 318 (24 800), 263 (25 800), 238 (34 500). FAB^+ m/z 491, $[M+H]^+$. (Calc. for $C_{13}H_{15}N_3O_2$: C, 63.66; H, 6.16; N, 17.13. Found: C, 63.58, H, 6.14; N, 17.10%).

3,6-Bis[6-(1,3-dihydroxy-4,4,5,5-tetramethylimidazolin-2-yl)-2-pyridyl]pyridazine 7b. 2,3-Bis(hydroxyamino)-2,3-dimethylbutane (0.268 g, 1.8 mmol) was condensed with 3,6-di(6-formyl-2-pyridyl)pyridazine **7a** (0.25 g, 0.86 mmol) in methanol (50 mL). The adduct **7b** precipitated, and was isolated by filtration (0.223 g, 47%). ^1H NMR (d_6-DMSO): δ 8.73 (s, 2H, CH pyridazine), 8.56 (d, 2H, $^3J=7.8$, H^3 pyridine), 8.07 (t, 2H, $^3J=7.7$, H^4 pyridine), 7,85 (s, 4H, OH), 7.77 (d, 2H, $3J=7.8$ Hz, H^5 pyridine), 4.81 (s, 2H, CH imidazoline), 1.14 (s, 12H, CH_3), 1.12 (s, 12H, CH_3). ^{13}C-{^1H} NMR (d_5-pyridine): δ 182.2, 163.4, 158.8, 152.8, 137.5, 125.2, 120.5, 92.86 (CH imidazoline), 67.7 (C_{quat} imidazoline), 24.8 (CH_3), 18.33(CH_3). IR (KBr): 3342s (ν_{OH}), 2983 m, 2931 m, 1592w, 1577 m, 1461s, 1372s, 1159s cm^{-1}. FAB^+ m/z 551, $[M+H]^+$; 535 $[M-O+H]$.

3,6-Bis[6-(3′-oxide-1′-oxyl-4′,4′,5′,5′-tetramethylimidazolin-2′-yl)-2-pyridyl]pyridazine 7c. An aqueous solution of sodium periodate (0.116 g, 0.54 mmol, in 20 mL water) was added to a suspension of compound **7b** (0.1 g, 0.18 mmol) in dichloromethane. The two phases were stirred together for one hour. The organic layers were then separated, and dried over magnesium sulfate. The solvent was removed under vacuum, and the blue solid was purified by chromatography (alumina CH_2Cl_2–MeOH 9:1), followed by a recrystallization in CH_2Cl_2–hexane, to obtain a blue compound (0.093 g, 95%). IR (KBr): 2996 m, 1587w, 1450 m, 1407 m, 1363s (ν_{NO}, 1186 m, 1141 m cm^{-1}. UV-Vis (CH_2Cl_2): λ/nm ($\varepsilon/M^{-1}\,cm^{-1}$) 574 (720) (n→π*, NO), 370 (26 800), 307 (31 800), 270 (38 700). FAB^+ m/z 545, $[M+H]^+$; 530 $[M-O+2H]$, 514 $[M-2O+2H]$, 498 $[M-3O+2H]$ (Calc. for $C_7H_8N_2O$: C, 61.75; H, 5.92; N, 20.57. Found: C, 61.62; H, 5.78; N, 20.38%).

General procedure for the synthesis of the copper(II) and nickel(II) complexes of ligands 1c and 6c. To a solution of ligand (0.01 g, $n=1$ equivalent for **6c**, 2 equivalents for **1c**) in CH_2Cl_2 (3 mL), was added a solution ($1.1n$) of the metal perchlorate salt in MeOH (3 mL). The mixture was stirred at room temperature for one night. The solvent was removed under vacuum, and the solid recrystallized in methanol–diethyl. CAUTION: Note that perchlorate salts should be handled carefully, in low quantities, used as hydrated salts, and never dehydrated under vacuum before use.

[2,9-Bis(4,4,5,5-tetramethylimidazoline 3-oxide 1-oxy 2-yl)-1,10-phenanthroline]copper(II) perchlorate 10. Yield 78%. IR (KBr): 2990w, 1573w, 1459 m, 1351s (ν_{NO}), 1320 m, 1106 (vs) cm^{-1}. UV-Vis (MeOH): λ/nm ($\varepsilon/M^{-1}\,cm^{-1}$) 755 (640), 680 (720) (n→π*, NO), 623 (660) (n→π*, NO), 329 (35 800), 268 (39 000), 217 (339 500). FAB^+ m/z 654, $[M-ClO_4+2H]^+$; 638 $[M-ClO_4-O]$, 622 $[M-ClO_4-2O]$, 554 $[M-2ClO_4+H]$, 538 $[M-2ClO_4-O+H]$, 522 $[M-2ClO_4-2O+H]$, 507 $[M-2ClO_4-3O]$ (Calc. for $C_{26}H_{30}Cl_2CuN_6O_{12}$: C, 41.47; H, 4.02; N, 11.16. Found: C, 41.25; H, 3.86; N, 10.95%).

[2,9-Bis(4,4,5,5-tetramethylimidazoline 3-oxide 1-oxy 2-yl)-1,10-phenanthroline]nickel(II) perchlorate 11. Yield 89%. IR (KBr): 2989w, 1562 m, 1458 m, 1355s (ν_{NO}), 1315w, 1098 (vs) cm^{-1}. UV-Vis (MeOH): λ/nm ($\varepsilon/M^{-1}\,cm^{-1}$) 768 (325), 694 (376) (n→π*, NO), 631 (310) (n→π*, NO), 331 (30 700), 271 (33 400), 240 (26 300), 211 (29 400). FAB^+ (m/z) 647, $[M-ClO_4]^+$; 631 $[M-ClO_4-O]$, 615 $[M-ClO_4-2O]$, 548 $[M-2ClO_4]$, 532 $[M-2ClO_4-O]$, 516 $[M-2ClO_4-2O]$. (Calc. for $C_{26}H_{30}Cl_2N_6NiO_{12}$: C, 41.74; H, 4.04; N, 11.23. Found: C, 41.59; H, 3.73; N, 11.02%).

Bis[2,6-bis(4,4,5,5-tetramethylimidazoline 3-oxide 1-oxy 2-yl)pyridine]copper(II) perchlorate 12. Yield 90%. IR (KBr): 2991 m, 1592 m, 1456 m, 1427 m, 1352s (ν_{NO}), 1175s, 1094 (vs) cm^{-1}. UV-Vis (MeOH): λ/nm ($\varepsilon/M^{-1}\,cm^{-1}$) 530 (3100) (n→π*, NO), 369 (32 700), 273 (28 900), 215 (38 400). FAB^+ m/z 942, $[M-ClO_4+2H]^+$; 926 $[M-ClO_4-O+2H]$, 912 $[M-ClO_4-2O+4H]$, 841 $[M-2ClO_4]$, 825 $[M-2ClO_4-O]$, 809 $[M-2ClO_4-2O]$, 793 $[M-2ClO_4-3O]$ (Calc. for $C_{38}H_{54}Cl_2CuN_{10}O_{16}$: C, 43.83; H, 5.23; N, 13.45. Found: C, 43.69; H, 5.17; N, 13.38%).

Bis[2,6-bis(4,4,5,5-tetramethylimidazoline 3-oxide 1-oxy 2-yl)pyridine]nickel(II) perchlorate 13. Yield 90%. IR (KBr) 2991w, 1591w, 1461 m, 1428 m, 1342s (ν_{NO}), 1178 m, 1099 (vs) cm^{-1}. UV-Vis (MeOH): λ/nm ($\varepsilon/M^{-1}\,cm^{-1}$) 764 (300), 575 (2000) (n→π*, NO), 369 (20 000), 210 (40 000). FAB^+ m/z 937 $[M-ClO_4+2H]^+$; 921 $[M-ClO_4-O]$, 905 $[M-ClO_4-2O]$, 836 $[M-2ClO_4]$, 820 $[M-2ClO_4-O]$, 804 $[M-2ClO_4-2O]$, 788 $[M-2ClO_4-3O]$ (Calc. for $C_{38}H_{54}Cl_2N_{10}NiO_{16}$: C, 44.03; H, 5.25; N, 13.51. Found: C, 43.87; H, 5.09; N, 13.41%).

Acknowledgements

The authors are pleased to acknowledge continued technical assistance from Richard Poinsot and Professor Antoine Herr from the Institut de Chimie des Matériaux de Strasbourg (IPCMS) and helpful discussions with Dr. Philippe Turek. We also warmly thank Dr. Dominique Luneau from the University Joseph Fourier in Grenoble for the determination of the crystal structure of compound **3c**, Dr. Francisco Romero for the parametrization of some of the magnetic behaviour, and Christophe Stroh for his help and advice during the close examination of the crystal packing. We also thank the crystallographic service of the Faculté de Chimie (Professor Jean Fischer and Dr. A. De Cian). This work was partially supported by the Centre National de la Recherche Scientifique, the Engineer School of Chemistry (ECPM) and by the Human Capital and Mobility Program of E.U. (Network: 'Magnetic Molecular Materials', No. ERBCHRXCT 920080).

References

1 J. H. Osiecki and E. F. Ullman, *J. Am. Chem. Soc.*, 1968, **90**, 1078; D. G. B. Boocock, R. Darcy and E. F. Ullman, *J. Am. Chem. Soc.*, 1968, **90**, 5945; E. F. Ullman, L. Call and J. H. Osiecki, *J. Org. Chem.*, 1970, **35**, 3623.
2 A. Caneschi, D. Gatteschi, R. Sessoli and P. Rey, *Acc. Chem. Res.*, 1989, **22**, 392.
3 A. Caneschi, D. Gatteschi, J. P. Renard, P. Rey and R. Sessoli, *Inorg. Chem.*, 1989, **28**, 1976; 3314.
4 A. Caneschi, D. Gatteschi, J. Laugier, P. Rey, R. Sessoli and C. Zanchini, *J. Am. Chem. Soc.*, 1988, **110**, 2795.
5 M. Tamura, Y. Nakasawa, D. Shiomi, K. Nozawa, M. Hosokoshi, M. Ishikawa, M. Takahashi and M. Kinoshita, *Chem. Phys. Lett.*, 1991, **186**, 401.
6 M. Kinoshita, P. Turek, M. Tamura, K. Nozawa, D. Shiomi, Y. Nakazawa, M. Ishikawa, M. Takahashi, K. Awaga, T. Inabe and Y. Maruyama, *Chem. Lett.*, 1991, 1225.
7 A. Rassat and P. Rey, *J. Chem. Soc., Chem. Commun.*, 1992, 1081; R. Chiarelli, M. A. Novak, A. Rassat and J. L. Tholence, *Nature* (*London*), 1993, **363**, 147.

8 A. Caneschi, F. Ferraro, D. Gatteschi, A. Le Liszin, M. A. Novak, E. Rentschler and R. Sessoli, *Adv. Mater.*, 1995, **7**, 476.
9 Y. Pei, O. Kahn, M. A. Aebersold, L. Ouahab, F. Le Berre, L. Pardi and J. L. Tholence, *Adv. Mater.*, 1994, **6**, 981; A. Lang, Y. Pei, L. Ouahab and O. Kahn, *Adv. Mater.*, 1996, **8**, 60.
10 E. Hernández, M. Mas, E. Molins, C. Rovira and J. Veciana, *Angew. Chem., Int. Ed. Engl.*, 1993, **32**, 88; J. Cirujeda, M. Mas, E. Molins, F. Lanfranc de Panthou, J. Laugier, J. G. Park, C. Paulsen, P. Rey, C. Rovira and J. Veciana, *J. Chem. Soc., Chem. Commun.*, 1995, 709.
11 T. Sugawara, M. M. Matsushita, A. Izuoka, N. Wada, N. Takeda and M. Ishikawa, *J. Chem. Soc., Chem. Commun.*, 1994, 1723; M. M. Matsushita, A. Izuoka, T. Sugawara, T. Kobayashi, N. Wada, N. Takeda and M. Ishikawa, *J. Am. Chem. Soc.*, 1997, **119**, 4369.
12 F. M. Romero, R. Ziessel, A. DeCian, J. Fischer and P. Turek, *New J. Chem.*, 1996, **20**, 919.
13 S. Nakatsuji and H. Anzai, *J. Mater. Chem.*, 1997, **7**, 2161.
14 A. J. Mancuso and C. Swern, *Synthesis*, 1981, 165.
15 O. Kocian, R. J. Mortimer and P. Beer, *Tetrahedron Lett.*, 1990, **31**, 5069.
16 J. Mendoza, E. Mesa, J.-C. Rodriguez-Ubis, P. Vazquez, F. Vögtle, P.-M. Windsheif, K. Rissanen, J.-M. Lehn, D. Lilienbaum and R. Ziessel, *Angew. Chem., Int. Ed. Engl.*, 1991, **30**, 1331.
17 J. E. Parks, B. E. Wagner and R. H. Holm, *J. Organomet. Chem.*, 1973, **56**, 53.
18 C. J. Chandler, L. W. Deady and J. A. Reiss, *J. Heterocycl. Chem.*, 1981, **18**, 599.
19 W. A. Butte and F. H. Case, *J. Org. Chem.*, 1961, **26**, 4690.
20 M. Lamchen and T. W. Mittag, *J. Chem. Soc. C*, 1966, 2300.
21 G. Ulrich, R. Ziessel, D. Luneau and P. Rey, *Tetrahedron Lett.*, 1994, **35**, 1211.
22 G. Ulrich and R. Ziessel, *Tetrahedron Lett.*, 1994, **35**, 1215.
23 E. F. Ullman, J. H. Osiecki, G. B. Boocock and R. Darcy, *J. Am. Chem. Soc.*, 1972, **94**, 704.
24 D. Luneau, F. M. Romero and R. Ziessel, *Chem. Commun.*, 1998, 551; *Inorg. Chem.*, 1998, **37**, 5078.
25 D. Luneau, J. Laugier, P. Rey, G. Ulrich, R. Ziessel, O. Legoll and M. Drillon, *J. Chem. Soc., Chem. Commun.*, 1994, 741.
26 C. K. Johnson, ORTEP, Report ORNL-5138, Oak Ridge National Laboratory, Oak Ridge, TN, 1976.
27 H. Oshio, A. Ohto, J. Fujisawa, T. Watanabe, T. Ito and K. Isobe, *Chem. Lett.*, 1994, 2353.
28 A. Caneschi, D. Gatteschi and P. Rey, *Prog. Inorg. Chem.*, 1991, **39**, 331.
29 A. Zheludev, V. Barone, M. Bonnet, B. Delley, A. Grand, E. Ressouche, P. Rey, R. Subra and J. Schweitzer, *J. Am. Chem. Soc.*, 1994, **116**, 2019.
30 G. R. Luckhurst and A. Hudson, *Mol. Phys.*, 1967, **13**, 409.
31 O. H. Griffith, P. J. Dehlinger and S. P. Van, *J. Membr. Biol.*, 1974, **15**, 159.
32 T. Mitsumori, K. Inoue, N. Koga and H. Iwamura, *J. Am. Chem. Soc.*, 1995, **117**, 2467.
33 R. Akabane, M. Tanaka, K. Matsuo, N. Koga, K. Matsuda and H. Iwamura, *J. Org. Chem.*, 1997, **62**, 8854.
34 B. Bleaney and D. K. Bowers, *Proc. R. Soc. London, Ser. A*, 1952, **214**, 451.
35 T. Sugano, M. Tamura and M. Kinoshita, *Synth. Metals*, 1993, 3305.
36 H. McConnell, *J. Chem. Phys.*, 1963, **39**, 1910.
37 A. El-Kasmi, D. Lexa, P. Mailard, M. Momenteau and J.-M. Savéant, *J. Phys. Chem.*, 1993, **97**, 6090.
38 H. Tamura, C. Iwakura and M. Tsunaga, *Electrochim. Acta*, 1973, **18**, 241.
39 T. Malinski, J. R. Fish, S. G. Swarts and M. D. Sevilla, *J. Phys. Chem.*, 1988, **92**, 3745.
40 D. Serve, *Electrochim. Acta*, 1975, **20**, 469.
41 D. Bartak, K. J. Klabunde, B. Henne and T. G. Groshens, *Inorg. Chem.*, 1981, **20**, 3629.
42 A. J. Bard, N. E. Tokel-Takvoryan and R. E. Hemingway, *J. Am. Chem. Soc.*, 1973, **95**, 6582.
43 J. M. Bobbit and C. L. Flores, *Heterocycles*, 1988, **27**, 509.
44 E. F. Ullman and D. G. B. Boocock, *J. Am. Chem. Soc.*, 1968, **90**, 6873.
45 B. Kalyanaraman, J. S. Hyde and J. Joseph, *Biochem. Biophys. Res. Commun.*, 1993, **192**, 926.
46 N. Tanaka and Y. Sato, *Bull. Chem. Soc. Jpn.*, 1968, **41**, 2059.
47 N. Tanaka and Y. Sato, *Bull. Chem. Soc. Jpn.*, 1968, **41**, 2064.
48 N. Tanaka and Y. Sato, *Electrochim. Acta*, 1968, **13**, 335.
49 OpenMoleN, Interactive Structure Solution, Nonius B.V., Delft, 1997.
50 D. T. Cromer and J. T. Waber, *International Tables for X-Ray Crystallography*, Kynoch Press, Birmingham, 1974, vol. IV, (*a*) Table 2.2b, (*b*) Table 2.3.1.

Paper 8/10044F